



Science Arts & Métiers (SAM)

is an open access repository that collects the work of Arts et Métiers Institute of Technology researchers and makes it freely available over the web where possible.

This is an author-deposited version published in: <https://sam.ensam.eu>
Handle ID: <http://hdl.handle.net/10985/11223>

To cite this version :

Alexander NIKITIN, Thierry PALIN-LUC, Andrey SHANYAVSKIY, Claude BATHIAS - Comparison of crack paths in a forged and extruded aeronautical titanium alloy loaded in torsion in the gigacycle fatigue regime - Engineering Fracture Mechanics p.1-14 - 2016

Any correspondence concerning this service should be sent to the repository

Administrator : scienceouverte@ensam.eu

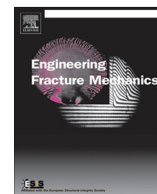




ELSEVIER

Contents lists available at ScienceDirect

Engineering Fracture Mechanics

journal homepage: www.elsevier.com/locate/engfracmech

Comparison of crack paths in a forged and extruded aeronautical titanium alloy loaded in torsion in the gigacycle fatigue regime

A. Nikitin^{a,b,*}, T. Palin-Luc^c, A. Shanyavskiy^{b,d}, C. Bathias^{a,1}

^a LEME, University Paris Ouest Nanterre La Defense, 50, rue de Serves, Ville-d'Avray 92410, France

^b MAI – National Research University, 4, Volokolamskoe Hwy, A-80, GSP-3, Moscow 125993, Russia

^c Arts et Metiers Paris Tech, I2M, CNRS, Universite de Bordeaux, Esplanade des Arts et Metiers, Talence 33405, France

^d Aviaregister, Air. Sheremetevo-1, PO Box 54, Moscow Reg., Chirkovskiy State, 141426, Russia

ARTICLE INFO

Article history:

Received 24 December 2015

Received in revised form 1 May 2016

Accepted 16 May 2016

Available online xxxx

Keywords:

Very-high cycle fatigue

Titanium alloy

Torsion

Crack initiation

Crack growth

Crack path

ABSTRACT

This paper discusses features of fatigue crack initiation and growth in an extruded and forged VT3-1 titanium alloy loaded in pure torsion in the gigacycle regime. Torsion fatigue tests were performed at 20 kHz up to a fatigue life of 10^9 cycles. It has been shown that regardless of the manufacturing process both surface and subsurface crack initiation may appear under ultrasonic torsion loads despite the fact that the maximum shear stress amplitude is located at the specimen surface. In the two cases cracks initiate on planes of maximum shear stress amplitude (mode II). After reaching a certain length the cracks turn and propagate in mode I. Surface crack initiation and growth mechanisms in VHCF regime are similar to HCF ones. Subsurface crack forms a typical “fish-eye” pattern on fracture surface with three different zones: (1) small crack growth in the plane of maximum shear stress, (2) crack growth on the plane of maximum normal stress with the formation of a quasi-flat failure surface covered by fretting debris, (3) crack branching under mixed mode loading conditions (I + II + III) with the formation of several secondary cracks. Subsurface crack initiation sites are located below the specimen surface (at a depth of approximately 200 μm) for both the forged and the extruded materials. Subsurface crack growth is observed on the failure surface as being less rough. The mechanisms of subsurface crack initiation seems to be similar to these observed under fully reversed tensile loads.

© 2016 Elsevier Ltd. All rights reserved.

1. Introduction

It has been demonstrated by many authors that the study of the fatigue properties of structural materials, such as steels, aluminum and titanium alloys, under torsion loading conditions is an important subject for industrial applications [1–4]. Many engineering components are subjected to complex loads involving bending, tension or torsion. Moreover, in the case of modern applications, such as cars, high-speed trains and aircraft engines, a very high number of in-service loading cycles can be experienced by components due to high loading rates or a very long life with low loading frequency [5–7]. The

* Corresponding author at: Institute for Computer Aided Design of Russian Academy of Science, Russia.

E-mail address: nikitin_alex@bk.ru (A. Nikitin).

¹ In memory.

Nomenclature

$\Delta\tau/2$	shear stress amplitude
N_f	number of cycles to failure
σ_D	fatigue strength under tensile loading
τ_D	fatigue strength under torsion loading
UTS	ultimate tensile strength
HV ₅₀₀	Vickers hardness with a load of 500 g

analysis of in-service loads for aeronautical applications [8,9] has shown that the fatigue life of compressor blades may reach more than 10^9 cycles (i.e. the very-high cycle fatigue (VHCF) regime). This fatigue regime has been under investigation since the beginning of the nineties [10,5]. In particular, the VHCF properties of structural materials have been investigated under axial push–pull loads, and different testing systems have been developed to reproduce different in-service loads and stress–strain conditions [11–13]. In recent years, VHCF investigations of metals under torsional loading conditions have become a subject of interest in the scientific community [13–15].

Results of ultrasonic fatigue tests on high-strength aluminum alloys have shown that torsional fatigue cracks in the VHCF regime have a qualitative similarity with crack in the HCF regime [12]. It was shown that crack initiation under torsion is located at the surface of specimen. The first stage of crack growth is found in the plane of maximum shear stress with the subsequent formation of a circumferential crack. However, a few years later, it was shown that under torsion loads in the VHCF regime subsurface cracks may also appear if the material contains non-metallic inclusions [16]. In this reference high-strength steel was studied up to a fatigue life of 10^9 cycles. For the case of surface initiation, the fatigue failure surfaces of 100Cr6 steel specimens show that, as in HCF, a typical “factory roof” pattern is observed [2,17]. ‘Factory roof’ pattern is a specific fracture surface morphology that is formed due to simultaneous torsion crack growth on several perpendicular planes. However, in the case of subsurface crack initiation, the initiation mechanism is more similar to uniaxial push–pull fatigue. In this case a “fish-eye” pattern is formed around an elongated non-metallic inclusion. The torsional fatigue crack does not show any significant branching and the “factory roof” failure surface is absent. For example 38MnSV5S steel shows surface crack initiation on the plane of maximum normal stress (45° to the specimen axis) [18] with subsequent propagation in an inclined plane (with respect to the specimen axis). There is also a tendency for the cracks to turn back to the plane experiencing the maximum shear stress.

No VHCF data concerning titanium alloys loaded under ultrasonic torsion is available in the literature. However, the study of Ti-alloys in torsional fatigue in the VHCF regime is a very interesting subject, because titanium is a defect free metal (with no inclusion or porosity) which has a relatively complex microstructure that may produce internal crack initiation, as seen in uniaxial push–pull fatigue [19–21]. The present paper is focused on the study of crack initiation mechanisms in the aeronautical titanium alloy VT3-1 under ultrasonic torsion in VHCF (10^6 – 10^9 cycles). Two main questions are discussed: (1) do VHCF torsion loads produce internal crack initiation in the VT3-1 titanium alloy? (2) are fatigue crack initiation and early stage crack growth in the VT3-1 alloy loaded in torsion similar to those observed for uniaxial push–pull loading conditions?

2. Experimental details and procedure

2.1. Materials

The material investigated in this work is the two phase ($\alpha + \beta$) titanium alloy VT3-1. This alloy is similar to the Ti-6Al-4V alloy and is commonly used in the Russian aircraft engine industry. Its standard chemical composition is presented in Table 1 (a detailed composition for the extruded and the forged VT3-1 alloys can be found in [13]).

Two sets of specimens were used. The first set was machined from a real compressor disk of Tu-154 aircraft engine D30, (see Fig. 1a). This disk was produced by forging and was used in service for 6000 flight cycles (takeoff–landing). An estimation of in-service time is approximately 18,000 h. After having been taken out of service, the compressor disk was examined by two non-destructive techniques (NDT): (i) ultrasonic NDT and (ii) alternating current field measurement. The aim of these methods is to detect cracks. The typical detectable crack length is 50 μm for ultrasonic NDT and about 5 mm for alternating current field. The results of these analyses did not show any noticeable fatigue damage due to the in-service loads and the disk was used to machine the ultrasonic fatigue specimens. The second set of specimens was machined from virgin extruded bars (Fig. 1b), produced by the “All Russian Institute of Light Alloys” with respect to their national standards [22]. The heat treatment of these bars was performed to obtain a fully lamellar microstructure (see Fig. 2) and mechanical properties close to those of the forged VT3-1 alloy, (see Table 2).

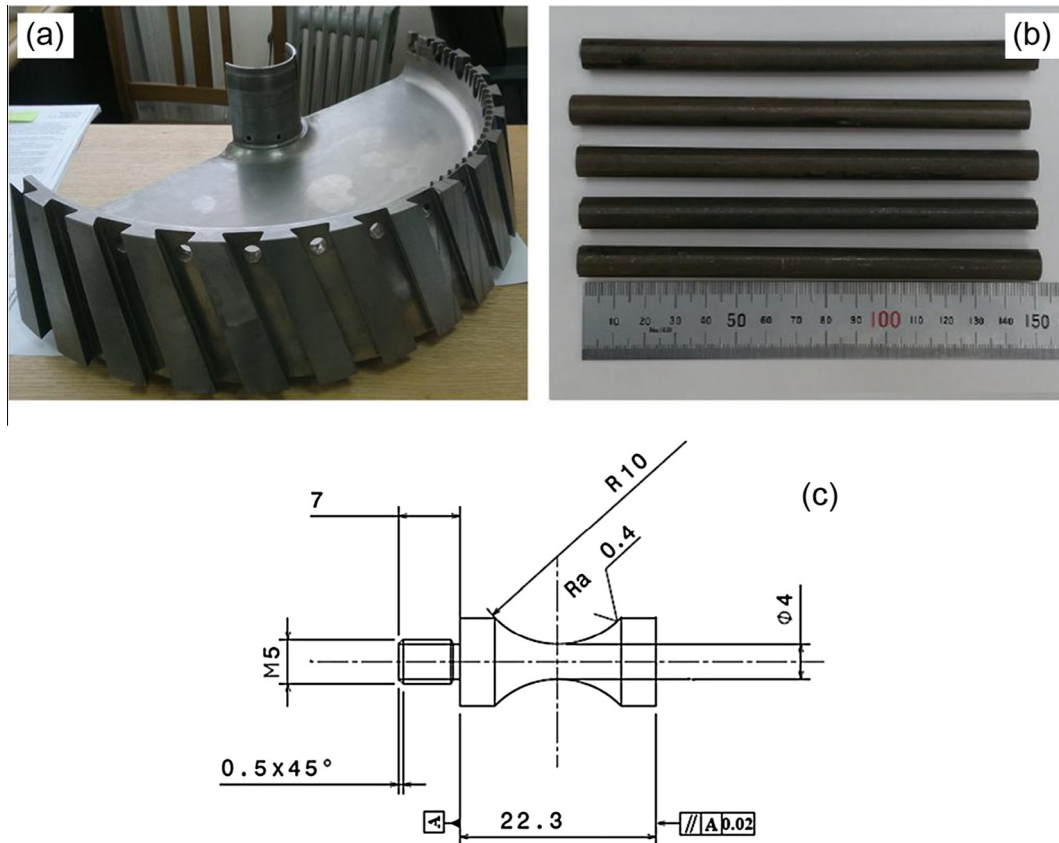
The geometry of the ultrasonic torsion specimens is the same for the two alloys and is shown in Fig. 1c.

The mechanical properties of these two materials were obtained via monotonic quasi-static tensile tests on flat specimens with a length of 75 mm and a thickness of 1 mm. The tests were conducted with a displacement rate of $0.075 \text{ mm min}^{-1}$. The

Table 1

Standard chemical composition of the VT3-1 titanium alloy (weight% with Ti as the balance).

Fe	C	Si	Cr	Mo	N	Al	Zr	O	H
0.2–0.7	<0.1	0.15–0.4	0.8–2	2–3	<0.05	5.5–7	<0.5	<0.15	<0.015

**Fig. 1.** Origin of the VT3-1 titanium alloy specimens, (a) compressor disk, (b) extruded bars and (c) the ultrasonic torsion specimen geometry, all the dimensions are in mm.

resulting mechanical properties are listed in Table 2. The dynamic modulus was determined at 20 kHz using a smooth cylindrical specimen. The extruded titanium alloy has slightly higher mechanical properties compared to the forged one, except its maximum elongation which is more than two times higher.

Fig. 2a and b shows the microstructure of the forged and extruded alloys respectively. At the grain-size scale these alloys have a similar fully lamellar microstructure with elongated alpha-platelets. However, the platelet size in the forged alloy is larger (with a width of approximately $w \approx 2 \mu\text{m}$ and a length of $l \approx 10\text{--}15 \mu\text{m}$) compared to the extruded alloy ($w \approx 1 \mu\text{m}$ and $l \approx 2\text{--}3 \mu\text{m}$). At the macroscopic scale the microstructure of the extruded titanium alloy is more homogeneous compared to the forged alloy (except some zones in the core of the bar). The microstructure of the forged titanium contains large zones of length up to several hundred micrometers with similar platelets morphology and crystallographic orientation. These zones have been observed in forged Ti-alloys and referred to as ‘macro-zones’ [23,24].

The micro-hardness of the two materials is approximately the same: 364 HV₅₀₀ for the forged alloy and 373 VH₅₀₀ for the extruded VT3-1 alloy. Micro-hardness measurements were done in a plane perpendicular to the longitudinal axis of the specimen along one diameter. The results show significant scatter for the forged alloy (see Fig. 2c). The observed difference between the min and max values is 44 HV₅₀₀ for points spaced 1.2 mm apart. For the extruded alloy this difference is less than 5 HV₅₀₀ (see Fig. 2d). This result can be associated with the difference microstructures observed for the forged and extruded alloys. Indeed, the micro-hardness is lower in the macro-zones because the platelets have a similar crystallographic orientation. The existence of “macro-zones” in the forged VT3-1 microstructure explains the large scatter observed in the micro-hardness values.

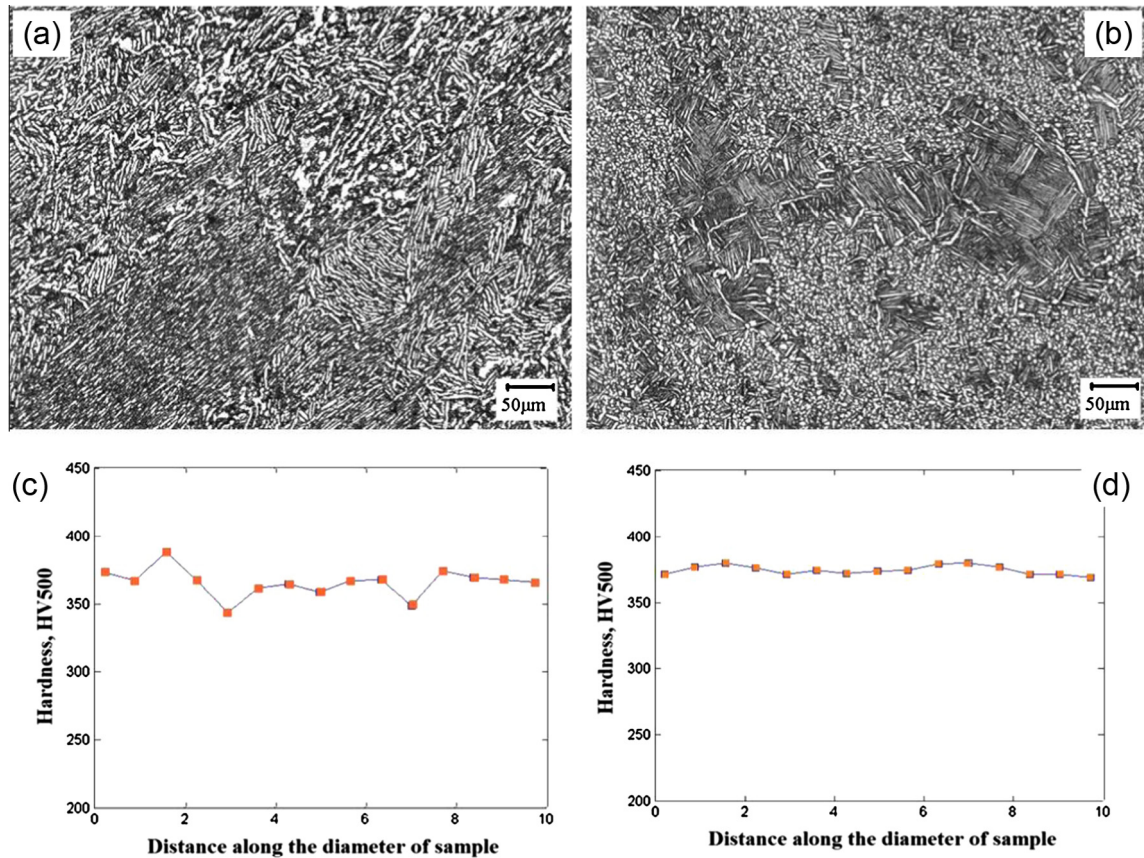


Fig. 2. Microstructure of the two VT3-1 alloys, (a) forged, (b) extruded and micro-hardness profiles along one diameter of the specimen cross section, (c) forged, (d) extruded.

Table 2

Mechanical properties of forged and extruded VT3-1 titanium alloys.

Process	Young's modulus, (GPa)	UTS (MPa)	Yield stress (MPa)	Maximum elongation (%)	Volumetric mass (kg m^{-3})	Dynamic modulus (GPa)
Forged	114	989	960	6	4500	116
Extruded	106	1107	1050	13	4500	110

2.2. Experimental details

Torsion fatigue tests were carried out on specimens, designed according to ultrasonic concepts applied to torsion [5,13] and taking into account the dynamic elastic properties of the materials at 20 kHz (Table 2). The specimens made from forged VT3-1 were cut from the rim part of the compressor disk. Their longitudinal axis was parallel to the rotation axis of the disk (Fig. 1a). The specimens made from extruded VT3-1 were machined from bars as illustrated in Fig. 1b. The geometry of the specimens is illustrated in Fig. 1c. The working section of these specimens was carefully mechanically polished with SiC paper from grades 600 to 1000.

Fatigue tests were carried out continuously (without pulse–pause) by using an in-house designed ultrasonic torsion system [13] up to fatigue failure or the run out limit of 10^9 cycles. The ultrasonic torsion testing machine is a resonance system based on a direct torsion piezoelectric converter that produces pure rotation. The system is continuously controlled by computer with high-performance feedback. Such high-quality control method allows an automatic detection of fatigue crack initiation by a resonance frequency drop of 4%. All tests were performed at room temperature with permanent cooling via a compressed dry-air jet. An infrared camera was used to monitor the surface temperature of certain specimens during the fatigue tests. The result shows that there is not a significant self-heating effect for either the forged or the extruded VT3-1 titanium alloys under ultrasonic torsion loads [13]. The calibration of the testing system was carefully carried out using an instrumented specimen. A strain gauge was glued on the specimen surface and a Vishay conditioning device (2210 type) with a large bandwidth (up to 100 kHz) was used. The results highlight a perfectly linear relationship between the voltage

applied to the piezoelectric converter and the measured strain amplitude. Fatigue crack initiation was detected by monitoring the resonance frequency drop. After each test the existence of a crack was verified with an optical microscope.

After cyclic loading and crack detection, each cracked specimen was broken in half using the following procedure. As previously discussed, titanium is a ductile material and significant plastic deformation may lead to the destruction (or damage) of the failure surface, if the specimen is simply broken by applying a tensile load. In order to minimize this risk the uncracked part of the specimen section was cut by wire electro-erosion. The electro-erosion wire was placed beside the fatigue crack so that surfaces of the crack lips are in the same plane as the wire (the specimen was typically inclined at 45° with respect to its longitudinal axis). After reducing the uncracked cross section of the specimen, it was cooled by immersion in liquid nitrogen and then subjected to a sharp shock in a direction so as to open the crack. The fatigue failure surfaces of all specimens were observed by scanning electron microscopy (SEM). Particular attention was paid to identify the crack initiation mechanisms.

3. Results

3.1. S–N curves for forged and extruded VT3-1 Ti-alloy

The fatigue test results (see in [Appendix A](#)) for both the forged ([Fig. 3a](#)) and the extruded ([Fig. 3b](#)) titanium alloys show that fatigue failure under pure torsion loads may occur well beyond 10^7 cycles. In spite of the limited number of tested specimens it is possible to plot a curve fitting the results in the S–N diagram. The experimental data were treated by least square method to obtain all the fitting lines without taking into account the run out specimens. It can be seen that the torsional fatigue strength of the extruded titanium alloy is higher than the forged one. This is in good agreement with the mechanical properties of these alloys determined via monotonic quasi-static tensile tests (see [Table 2](#)). Note that the two S–N curves have a high slope in the VHCF regime. The decrease in the fatigue strength with the number of loading cycles is more pronounced for the torsional loading mode compared to the results of uniaxial tension-compressing tests [[25](#)].

3.2. Crack paths observed on the specimen surface

Initial observations were carried out on the surface of the specimens (see [Fig. 4](#)). Fatigue cracks observed on the specimen surface have two clear stages for both the forged and the extruded materials. The first stage of crack propagation is observed on a plane experiencing the maximum shear stress amplitude, i.e. the planes perpendicular or parallel to the specimen's longitudinal axis. The second stage is when the crack becomes longer, it bifurcates to propagate in Mode I on the plane(s) of maximum normal stress (i.e. on planes having an angle of 45° with respect to the specimen's longitudinal axis).

For the two materials the main crack propagates on the plane of maximum normal stress up to the final length corresponding to the end of the test. Nonetheless, several bifurcations onto the maximum shear stress planes were observed even for long torsion cracks (see [Fig. 4](#)). The crack path for the extruded titanium alloy is less perturbed compared to the crack path on the forged material. In this case several parallel cracks can be observed on planes experiencing the maximum normal stress (see [Fig. 4](#)). Crack growth under torsion loads appears to be quite sensitive to the material microstructure. Indeed via comparing the surface crack path of the extruded and forged titanium alloys it can be seen that crack branching is more frequent in the forged titanium alloy which has a less homogeneous microstructure compared to the extruded alloy. In the forged alloy the crack path due to torsion loads is more tortuous (“zigzag like” due to alternative bifurcation between mode I and mode II propagation). Furthermore, it should be noted that macroscopically, crack growth in the plane of maximum normal stress may be found in a single plane, as well in two perpendicular planes at the same time (X-type cracks, see [Fig. 4](#)). This is similar to the HCF regime observed for many metals [[26](#)].

3.3. Crack initiation mechanism

Observations of the fatigue failure surfaces (after opening the specimens) have shown that both surface and subsurface crack initiation is possible for both titanium alloys under investigation. This result is very important in torsion because internal crack initiation is observed despite the fact that the maximum shear stress is located at the surface of the specimen. The transition from surface to subsurface crack initiation was found to occur at approximately 10^8 cycles for both alloys.

3.3.1. Surface crack initiation

For the case of surface crack initiation, macroscopically the final crack front on the failure surface has an elliptical shape on the plane of maximum normal stresses, as per the HCF regime. The smaller axis of the ellipse is always orientated toward the centre of the specimen for both the forged and extruded titanium alloys (see [Fig. 5a](#) and [b](#)). The failure surface for the extruded titanium alloy is less rough compared to the forged material. The crack path in the forged titanium alloy has a very complex morphology due to the non-homogeneous microstructure that makes it difficult to clearly define the transition between different crack propagation stages. However for the case of the extruded titanium alloy with a more homogeneous microstructure three clear stages of crack propagation can be highlighted: (1) small crack growth in a plane of maximum shear stress, (2) crack growth in a plane of maximum normal stress, with the formation of a quasi-flat failure surface covered by fretting debris, (3) and crack branching under mixed mode loading (I + II + III) with the forming of several cracks in alternative planes (perpendicular to the main crack propagation plane).

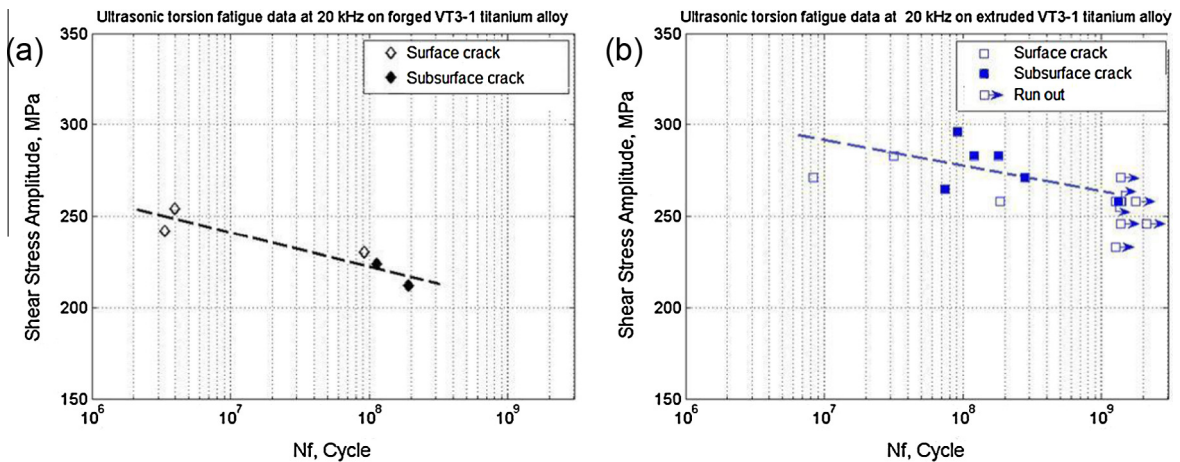


Fig. 3. SN-curve for (a) forged and (b) extruded VT3-1 titanium alloy under torsion in VHCF regime.

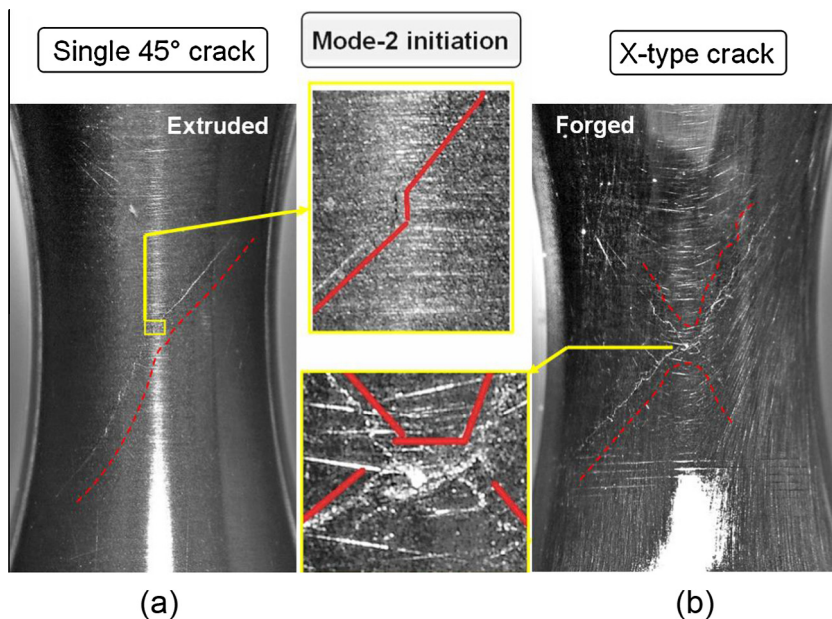


Fig. 4. Surface crack path (optical microscopy) on (a) extruded and (b) forged VT3-1 Ti-alloy.

The zone of first stage crack growth is very small and limited by several tens of micrometers, (Fig. 5c and d). Moreover, due to the Mode II cracking this first zone is significantly destroyed by shear and friction, which makes it impossible to determine a specific feature of the microstructure at the origin of the crack initiation. This first zone is surrounded by separated areas with a crumpled failure surface that are formed due to contact at the crack edges. The same zones, destroyed by contact because of the fully reversed loads, were observed on the forged titanium alloy. The crumpled zones are located at a distance of about 100 μm from the crack initiation site. Note that the non-crumpled failure surface is covered by small spherical particles that are mainly located in individual dimples as it can be seen later. Beyond the crack initiation area with the crumpled zones, the torsion crack propagates on a plane of maximum normal stress with the formation of a quasi-flat surface with slight perturbation by ‘river-marks’. Far from the crack initiation site, at a distance of about 300–400 μm , an initial crack branch appears that can be seen as “river-like” marks on the failure surface, (Fig. 6).

These branches are visible all along the crack front as inclined “wings”. These features of failure surface morphology are formed due to crack propagation in a series of parallel planes, orientated at 45° with respect to the specimen longitudinal axis. They show that active torsion crack branching can be observed in the bulk of material and not only at the specimen surface. These “torsion wing” marks are visible up to the final crack front when the fatigue test was stopped.

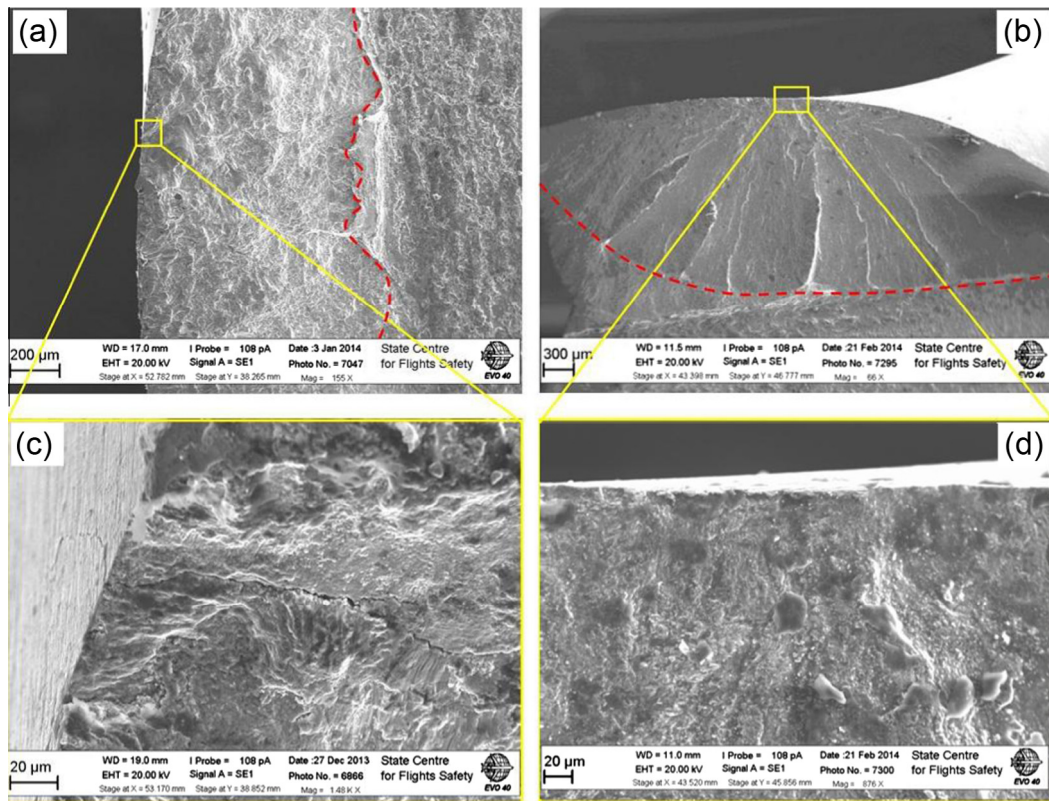


Fig. 5. Surface crack initiation (a and b) macroscopic views of the forged and extruded alloys respectively (c and d) zoomed views of the initiation sites for the forged and extruded alloys respectively.

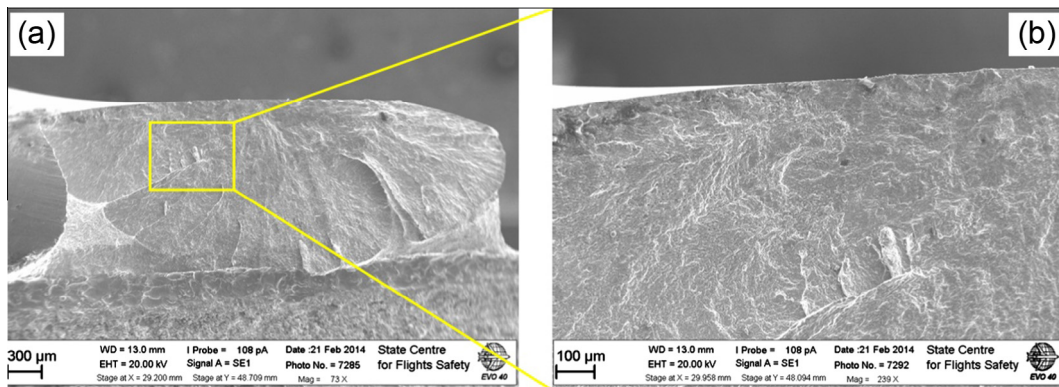


Fig. 6. 'River-like' marks for surface initiation in the extruded titanium alloy (a) overview of the failure surface and (b) zoomed view at the beginning of branching.

3.3.2. Subsurface crack initiation

For the case of subsurface crack initiation the shape of the final macroscopic crack front also has an elliptical shape on the plane of maximum normal stress, as per surface crack initiation. The small axis of this ellipse is also orientated toward the center of the specimen for the two titanium alloys (see Fig. 7(a and b)).

The orientation of the torsion cracks is different from that observed for subsurface cracks in high-strength steel loaded in ultrasonic torsion, in which the small axis was orientated parallel to the specimen surface [14]. In the investigated titanium alloys the crack initiation site is located in the bulk of the material at a distance of approximately 200 µm from the specimen surface. Subsurface crack initiation produces a clear "fish-eye" pattern on the failure surface. The "fish-eye" pattern is clearer for the extruded titanium alloy compared to the forged material. For the forged alloy the morphology of the failure surface is

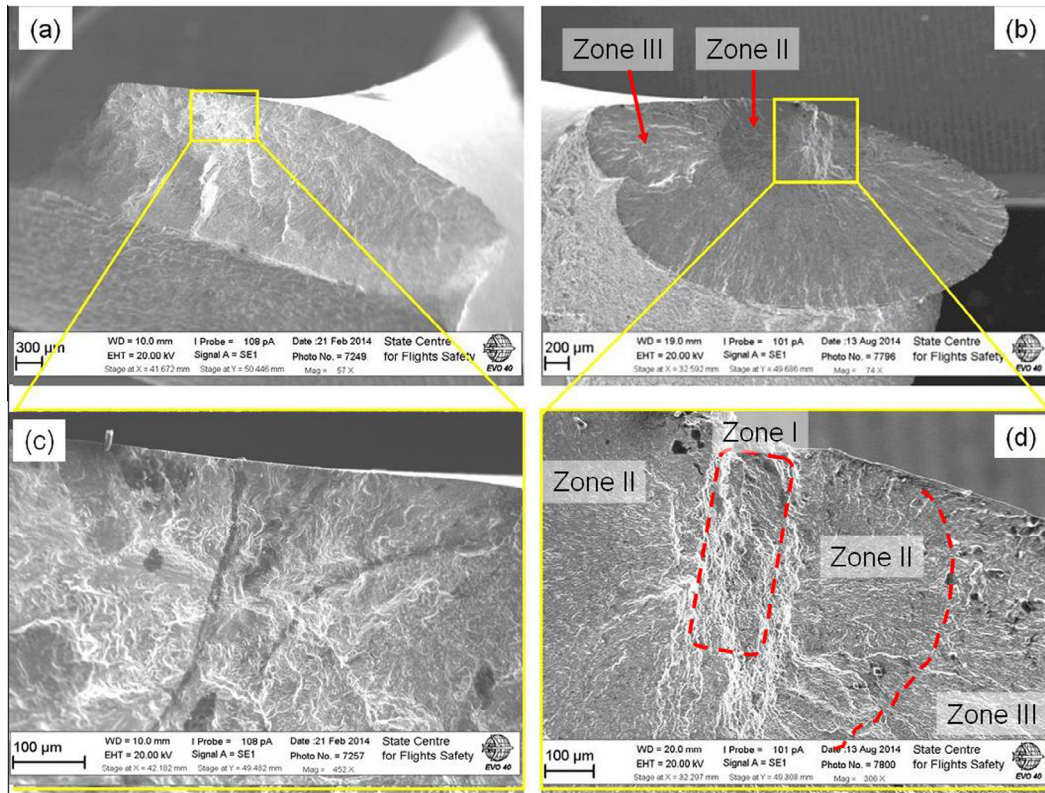


Fig. 7. Fatigue failure surfaces with subsurface crack initiation: macroscopic view for (a) forged and (b) extruded Ti-alloy, and zoomed views of the crack initiation area for (c) forged and (d) extruded alloys.

more perturbed by the microstructure. Nonetheless, three different zones related to subsurface crack growth can be observed on the fracture surface for both forged and extruded titanium alloys: (1) a zone of internal crack initiation and early growth on a plane of maximum shear stress, (2) the subsurface stage of the torsional fatigue crack propagation and (3) a rough failure surface zone where the torsion crack reaches the specimen surface. As previously discussed for surface crack initiation the first zone is related to crack initiation and early growth (Stage I, mode II). The small crack then bifurcates into mode I (stage II), like in the HCF regime. The size of the first zone is larger for the extruded titanium alloy compared to the forged one. For some extruded specimens this size can reach up to hundred micrometers. In the case of the forged titanium alloy this first zone is significantly smaller and does not exceed several tens of micrometers. This zone is damaged by friction wear due to shear for the two alloys, which makes it impossible to identify any microstructural features related to crack initiation. Close to this first zone small spherical particles are observed (Fig. 8d). Unlike the case of surface crack initiation, for subsurface cracks these particles are located in elongated grooves (Fig. 8b). Similar spherical particles and grooves were found in both materials for subsurface crack initiation.

A second remarkable feature of the failure surfaces for subsurface initiation is the clear transition from subsurface (zone II) to surface (zone III) crack propagation (see Fig. 7a and b). The subsurface crack propagation stage produces a smoother failure surface that is clearly seen as a “darker” area. When the torsion crack reaches the specimen surface the failure surface becomes rougher and its color is clearer. “Torsion wings”, already observed for surface crack initiation were also observed for subsurface crack initiation. It is important to outline that these “torsion wings” are formed during the subsurface crack propagation stage and continue to grow when the torsion crack reaches the specimen surface. Nonetheless, branching is less active in the case of subsurface crack initiation compared to surface initiation. This means that for subsurface crack initiation, the growth of several cracks in 45° planes is also possible, but limited. It is interesting to point out, that for high strength steel [16], a fracture surface with internal crack initiation does not show branching patterns (no 45° “wings”).

4. Discussion

This paper introduces the first detailed results concerning the fatigue behavior of titanium alloys under pure torsional loads in the gigacycle fatigue regime. The analysis of the S–N curves (Fig. 3) has shown that the fatigue strength of the extruded VT3-1 alloy is approximately 50 MPa greater than the forged titanium alloy whereas the S–N curve slopes are almost the same for the two alloys. No “run-out” result were obtained for the forged titanium alloy while for the extruded material

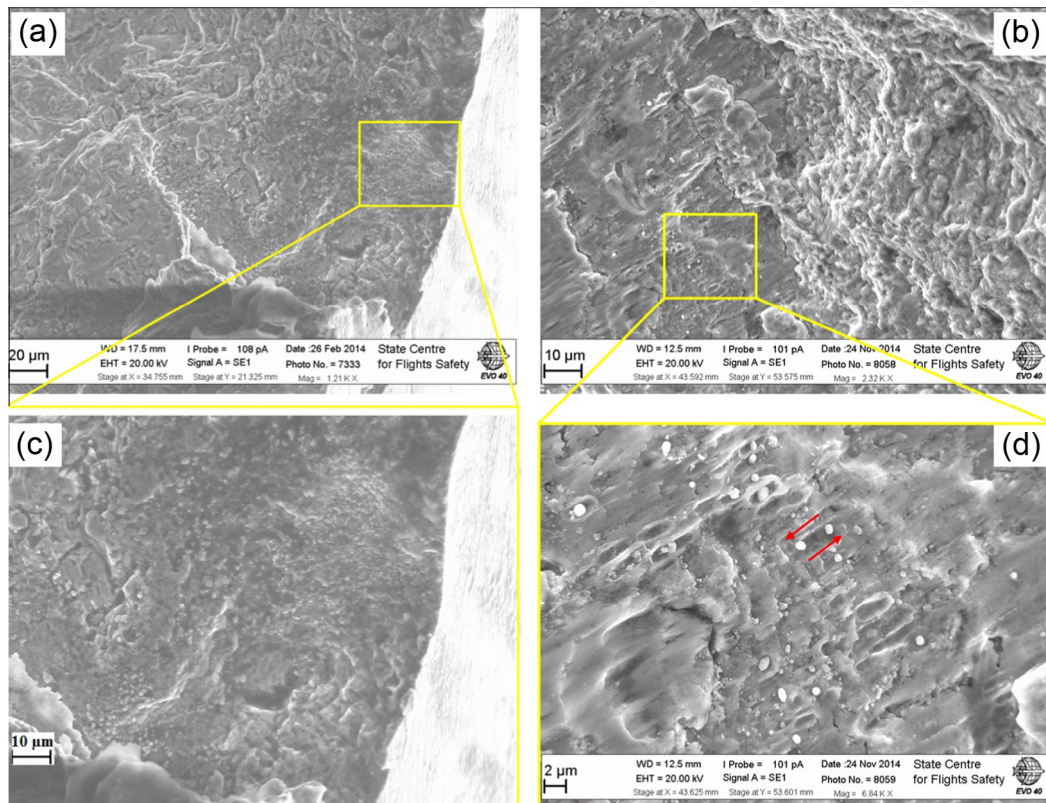


Fig. 8. Spherical particles in the case of (a) surface (b) and subsurface crack initiation.

several not-failed specimens were obtained with a shear stress amplitude of $\Delta\tau/2 = 246$ MPa. For the forged VT3-1 titanium alloy a longer fatigue life of $N_f = 1.93 \times 10^8$ cycles, was obtained for an applied shear stress amplitude of $\Delta\tau/2 = 212$ MPa. Unfortunately there are no other results of torsion VHCF tests on titanium alloy in literature. Consequently in order to compare our results with data available in literature [5] we have to use an equivalent stress. Some authors have shown [27] that Von-Mises equivalent stress could be used to compare torsion and tensile results in HCF. By using the Von-Mises equivalent stress, our results can be compared to uniaxial push–pull results for the forged Ti-6246 [5] obtained at 20 kHz. Uniaxial tensile fatigue strength of the Ti-6246 alloy at 10^9 cycles varies from $\sigma_D = 325$ to 490 MPa depending on the microstructure. Thus, as a first approximation by assuming the Von Mises relation is valid for the gigacycle fatigue strength, the expected range for the fatigue strength at 10^9 cycles in torsion is $\tau_D = 187$ to 283 MPa. This is in good agreement with the results of this study on VT3-1 titanium alloy. Furthermore, comparing the VHCF results in torsion with previously obtained push–pull results on forged [28] and extruded [29] VT3-1 titanium alloys [25] it can be shown that the slope of the S–N curves in torsion is greater than the slope for uniaxial push–pull loads for the two alloys. This means that VT3-1 titanium is more sensitive to the shear stress amplitude than the normal stress amplitude.

The observation of torsion cracks on the specimen surfaces has shown that the first stage of crack growth is on the plane of maximum shear stress. This is typical for ductile metals. In the case of two-phase $\alpha + \beta$ titanium alloys the hexagonal alpha-phase has a higher capacity to accommodate plastic sliding than the beta phase (BCC). Therefore, at the very first stage of fatigue crack initiation and early growth, when the crack length is about the same order of magnitude as the grain size, fatigue damage accumulation is determined by the capacity of alpha-phase to plastically deform. Thus, the VHCF fatigue resistance of titanium alloys under torsion loads can be significantly dependent of the features of alpha-platelets (geometry, orientation, clustering and etc.)

SEM observations on fracture surface show surface and subsurface crack initiations in the two materials. For the forged titanium alloy as well as the extruded VT3-1 alloy, the crack initiation site is found in the plane of maximum shear stress regardless the initiation mode. These planes are covered by spherical particles occurring in individual dimples. The spectral analysis of these spherical particles shows that they have the same chemical composition as the titanium alloy. The geometry of the dimples, where these particles are located, shows that there was no significant relative linear displacement of the crack lips during the formation of the particles (see Fig. 8a). Indeed, the shape of dimples is close to a hemisphere. The mechanism of formation of these particles seems to be similar to that proposed by A. Shanyavskiy [30] for bi-axial loads. Under torsion loads small modifications to the proposed mechanism [30] should be made as illustrated in Fig. 9.

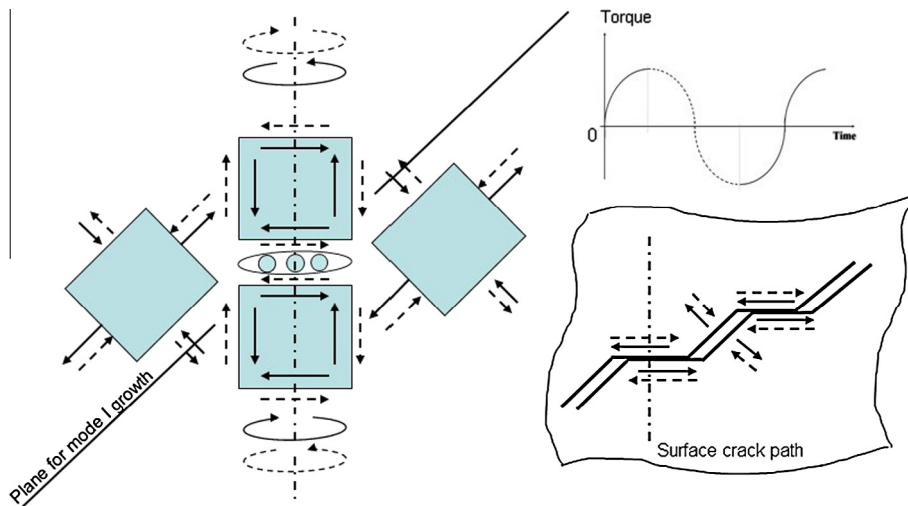


Fig. 9. Schematic illustration for the formation of spherical particles under cyclic torsion loads.

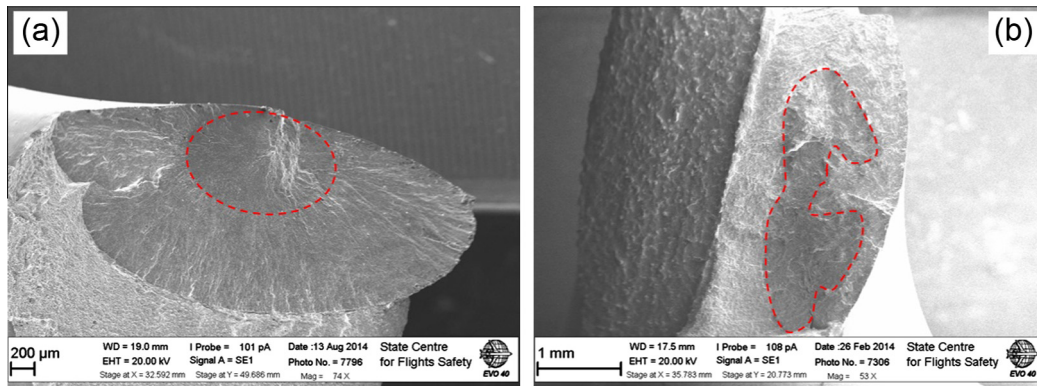


Fig. 10. Subsurface crack initiation with “fish-eye” failure surfaces in torsion, (a) the extruded VT3-1 alloy and (b) the forged alloy.

The main idea behind the explanation is the local contact between the crack lips on the local plane (at meso-scale) of maximum shear stress when the long fatigue crack propagates under tensile stresses on the macroscopic plane experiencing the maximum normal stress. Due to the local loading conditions, the spherical particles are formed under a mixed mode (II + III) loading condition. The relative opening displacement of the lips in contact is limited and the cyclic loading produces particles formed in individual dimples (similar to fretting fatigue). The destruction of the crack initiation site by the previously described mechanism makes it impossible to study in detail the surface crack initiation mechanism in the VT3-1 titanium alloy under VHCF torsion loads. Concerning subsurface crack initiation, the crack initiation sites are usually located at a distance of about 200 μm from the surface for the two titanium alloys. Moreover, for the forged titanium alloy it appears that the subsurface crack initiation site can be observed at different distances from the surface. The perturbed failure surfaces do not allow the confirmation of this, but some elements of the failure surface morphology make the assumption possible. It is clearly seen from the failure surfaces of the extruded titanium alloy, that the color of the failure surface is not the same for the subsurface and the surface crack propagation stages. The darker color is for subsurface crack propagation stage. As can be seen in Fig. 10 two zones with different colors can be distinguished.

One zone surrounds the surface crack initiation site, which is on a plane of maximum shear stress and a second darker zone can also be seen. This zone is defined by the dotted red line in Fig. 10. The second zone is surrounding a feature of the fracture surface that is similar to that found for subsurface crack initiation in the forged VT3-1 alloy. This implies that for the forged titanium alloy, the complex structure containing macro-zones can have a very strong influence on crack initiation in torsion. For the case of subsurface crack initiation, the crack opening displacement is limited and the areas close to the crack initiation zone remain in contact during fatigue crack growth. This can be clearly seen on the failure surface where spherical

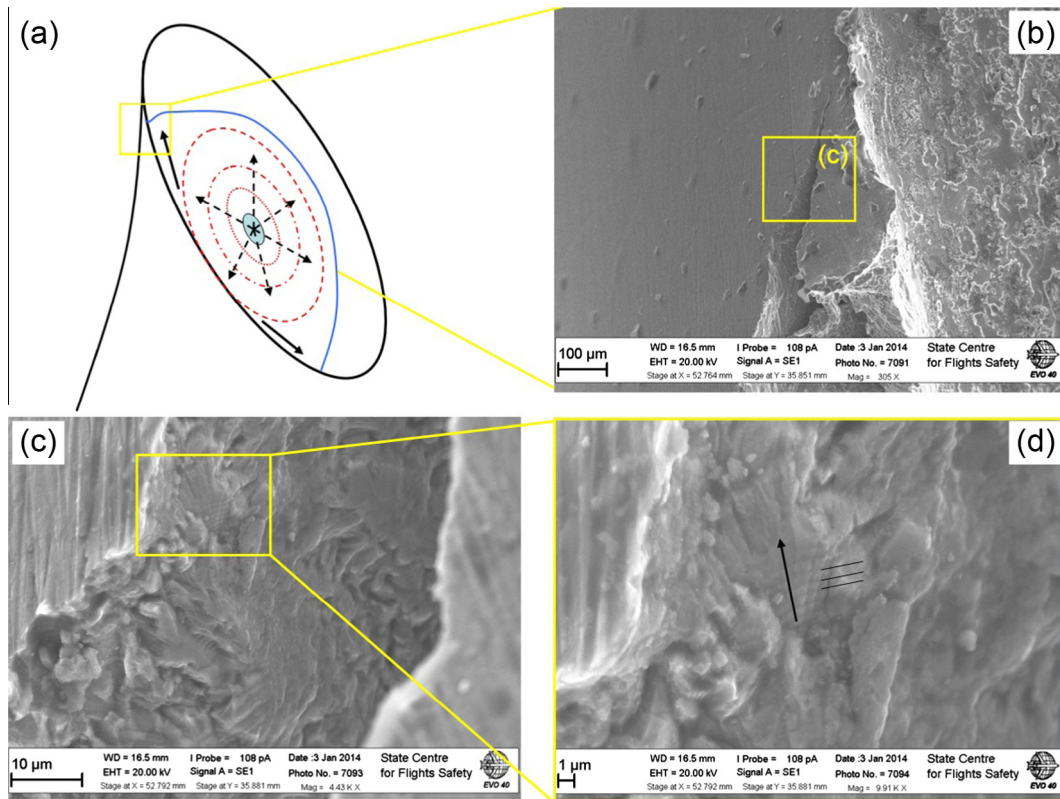


Fig. 11. The forged VT3-1 alloy, crack propagation marks close to the crack tip showing local crack growth from the bulk to the surface.

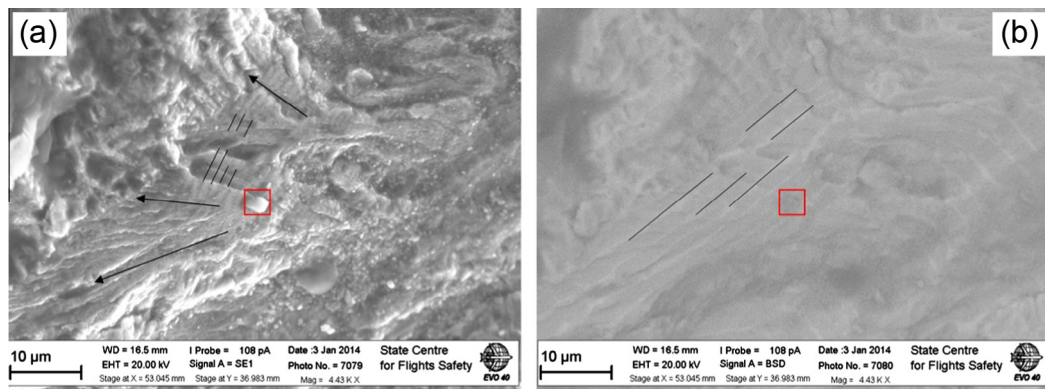


Fig. 12. Incremental fatigue crack propagation marks observed by SEM (a) in secondary electron mode and (b) observed at the same location in back scattered electron mode.

particles still exist (similar to the crack initiation zone) but they are located in elongated grooves (Fig. 8b). The groove geometry indicates that spherical particles were formed in the presence of important relative linear displacement between the crack lips. Like in the crack initiation zone, these particles have the same chemical composition as the VT3-1 titanium alloy.

Far from the crack initiation site, where the failure surface is destroyed by friction, the morphology of the crack path is clearer and subsurface branching can be detected. For both titanium alloys branching starts before the internal crack reaches the specimen surface. This result is different from the result obtained for the Ti–6Al–4V alloy in the HCF regime by Shiozawa et al. [31].

In reference [31] fully reversed torsion fatigue tests were carried out on the Ti–6Al–4V titanium alloy in the HCF regime at a loading frequency of 10 Hz. It was shown that in HCF a torsion crack first grows in the depth of the material and afterwards it branches at the surface without growing deeper. In the case of ultrasonic torsion testing on the VT3-1 titanium alloy the crack tip position versus the number of cycles was not monitored and the crack shape was reconstructed based on the failure surface pattern. SEM observations show that “torsion wings” appear before any modification of the failure surface roughness. These can be seen as a slight difference in the color of the failure surface. “Torsion wing” marks are formed as a result of the competition between cracks growing onto two planes of maximum normal stress. The interaction of two cracks growing in two perpendicular planes forms an inclined plane on the global macroscopic failure surface. This mechanism is similar for surface and subsurface crack initiation.

After crack branching, a very clear transition from the subsurface to the surface propagation regime can be outlined on the failure surface. This transition is characterized by a clear difference in the color of the surface. When the internal crack front reaches the specimen surface the stress intensity factor increases significantly. Consequently the shape of the crack front changes quickly (surface crack propagation is quicker than propagation in the bulk of the material). This is confirmed by SEM observations showing that some subsurface small cracks were growing from the bulk material toward the surface of the specimen (Fig. 11). This can be concluded based on the analysis of certain marks on the failure surface (see Fig. 11d). These marks are not alpha-platelets of the VT3-1 alloy; this was deduced from SEM image taken in the back scattered electron mode at the same location (see Fig. 12).

These marks were formed as a result of incremental torsional crack growth. Similar zones showing incremental crack propagation marks were found in other locations. They show the crack propagation direction “from the bulk toward the surface” (see Fig. 11).

5. Conclusion and prospects

Based on experimental results obtained at 20 kHz under pure ultrasonic torsion in the gigacycle fatigue regime, the following conclusions can be made:

- (1) The S–N curves of the VT3-1 titanium alloy loaded in torsion ($R = -1$) have a more significant slope, compared to the results published for fully reversed tension. The Von Mises equivalent stress seems to be suitable for linking the tensile and torsional VHCF strengths for the forged, but not for extruded VT3-1 Ti-alloys. Regardless of the manufacturing process (forging or extrusion) both surface and subsurface crack initiation was observed. Subsurface crack initiation was observed for specimens that failed at greater fatigue lives. The transition from surface to subsurface crack initiation was found to occur later than the transition observed for uniaxial push–pull loads: about 10^8 cycles for torsion and 10^6 cycles for uniaxial loads. “Fish-eye” failure surfaces were observed for torsion loads in the VHCF regime, similar to those often reported in the literature for the uniaxial loading condition.
- (2) Qualitatively, failures generated under torsional loads in VHCF are similar to the HCF results, except there is the additional possibility in VHCF regime of internal cracks (fish-eye even without inclusion) and the possibility to branch.
- (3) A sort of branching ‘threshold’ or critical crack length can be found on the failure surface, beyond which a torsion crack shows several branches to another 45° plane of maximum normal stress. Concerning internal cracks, initiation and early crack growth is in Mode II like in the HCF regime but at the surface. Bifurcation and growth onto a plane of maximum normal stress occurs before the crack reaches the specimen surface. Further crack growth occurs along the specimen surface.

Additional investigations should be carried out on other titanium alloys to determine if the proposed conclusions can be generalized to other Ti-alloys.

Appendix A

Results of ultrasonic torsional fatigue tests on forged VT3-1 titanium alloy

Specimen number	Shear stress amplitude (MPa)	Nb of cycles	Crack initiation location (surface or subsurface)
Forged 1	254	3.96×10^6	Surface
Forged 2	242	3.37×10^6	Surface
Forged 3	230	9.22×10^7	Surface
Forged 4	224	1.13×10^8	Subsurface
Forged 5	212	1.93×10^8	Subsurface

Results of ultrasonic torsional fatigue tests on extruded VT3-1 titanium alloy

Specimen number	Shear stress amplitude (MPa)	Nb of cycles	Crack initiation location (surface or subsurface)
Extruded 1	271	8.365×10^6	Surface
Extruded 2	283	3.17×10^7	Surface
Extruded 3	265	7.357×10^7	Subsurface
Extruded 4	296	9.05×10^7	Subsurface
Extruded 5	283	1.211×10^8	Subsurface
Extruded 6	283	1.786×10^8	Subsurface
Extruded 7	256	1.837×10^8	Surface
Extruded 8	271	2.819×10^8	Subsurface
Extruded 9	271	1.37×10^9	Subsurface
Extruded 10	246	1.364×10^9	Run out
Extruded 11	246	2.114×10^9	Run out
Extruded 12	258	1.255×10^9	Run out
Extruded 13	258	1.378×10^9	Run out
Extruded 14	258	1.758×10^9	Run out
Extruded 15	271	1.367×10^9	Run out
Extruded 16	230	1.28×10^9	Run out

References

- [1] Shimamura Y, Narita K, Ishii H, Tohgo K, Fujii T, Yagasaki T, et al. Fatigue properties of carburized alloy steel in very high cycle regime under torsional loading. *Int J Fatigue* 2014;60:57–62. [10.1016/j.ijfatigue.2013.06.016](https://doi.org/10.1016/j.ijfatigue.2013.06.016).
- [2] Tschegg EK, Stanzl-Tschegg SE, Mayer HR. High frequency method for torsion fatigue testing. *Ultrasonics* 1993;31(4):275–80.
- [3] Pokluda J, Pippan R, Vojtek T, Hohenwarther A. Near-threshold behavior of shear-mode fatigue cracks in metallic materials. *FFEMS* 2014;37(3):232–54.
- [4] Vojtek T, Pokluda J, Sanderá P, Hornikova J, Hohenwarther A, Pippan R. Analysis of fatigue crack propagation under mixed mode II + III in armco iron. *Int J Fatigue* 2015;76:47–52.
- [5] Bathias C, Paris PC. *Gigacycle fatigue in mechanical practice*. New York: Dekker; 2005. ISBN-10: 0824723139.
- [6] Shanyavskiy A. Modeling of metals fatigue cracking. Synergetic in aviation, Monography, Ufa, Russia; 2007.
- [7] Palin-Luc T, Perez-Mora R, Bathias C, Dominguez G, Paris PC, Arana J-L. Fatigue crack initiation and growth on a steel in the very high cycle regime with sea water corrosion. *Engng Fract Mech* 2010;77:1953–62.
- [8] Nicholas T. Critical issues in high cycle fatigue. *Int J Fatigue* 1999;21:S221–31. [http://dx.doi.org/10.1016/S0142-1123\(99\)00074-2](http://dx.doi.org/10.1016/S0142-1123(99)00074-2).
- [9] Shanyavskiy A. Very-high-cycle-fatigue of in-service air-engine blades, compressor and turbine. *Phys Mech Astron* 2014;57(1):19–29.
- [10] Sakai T. Review and prospects for current studies on very high cycle fatigue of metallic materials for machine structural use. *J Solid Mech Mater Eng* 2009;3(3):425–39. <http://dx.doi.org/10.1299/jimmp.3.425>.
- [11] Bathias C. Piezoelectric fatigue testing machines and devices. *Int J Fatigue* 2006;28(11):1438–45. <http://dx.doi.org/10.1016/j.ijfatigue.2005.09.020>.
- [12] Mayer H. Ultrasonic torsion and tension-compression fatigue testing: measuring principles and investigations on 2024-T351 aluminium alloy 28(11): 1446–1455. <http://dx.doi.org/10.1016/j.ijfatigue.2005.05.020>.
- [13] Nikitin A, Palin-Luc T, Bathias C. A new piezoelectric fatigue testing machine in pure torsion for ultrasonic gigacycle fatigue tests: application to forged and extruded titanium alloys. *FFEMS* 2015;38(11):1294–304. <http://dx.doi.org/10.1111/ffe.12340>.
- [14] Mayer H, Schuller R, Karr U, Irrasch D, Fitzka M, Hahn M, et al. Cyclic torsion very high cycle fatigue of VDSiCr spring steel at different load ratios 2015;70:322–7. <http://dx.doi.org/10.1016/j.ijfatigue.2014.10.007>.
- [15] Ishii H, Tohgo K, Fujii T, Yagasaki T, Harada M, Shimamura Y, et al. Fatigue properties of carburized alloy steel in very high cycle regime under torsion loading. *Int J Fatigue* 2014;60:57–62. <http://dx.doi.org/10.1016/j.ijfatigue.2013.06.016>.
- [16] Xue HQ, Bathias C. Crack path in torsion loading in very high cycle fatigue regime. *Engng Fract Mech* 2010;77:1866–73. <http://dx.doi.org/10.1016/j.engfractmech.2010.05.006>.
- [17] Tanaka K. Small crack propagation in multiaxial notch fatigue, proceedings of Crack Path 2012; 2012. p. 31–45.
- [18] Marines-García I, Doucet JP, Bathias C. Development of a new device to perform torsional ultrasonic fatigue testing. *Int J Fatigue* 2007;29:2094–101. <http://dx.doi.org/10.1016/j.ijfatigue.2007.03.016>.
- [19] Nikitin A, Palin-Luc T, Shanyavskiy A, Bathias C. Fatigue cracking in bifurcation area of titanium alloy at 20 kHz. In: Proceedings crack path; 2012. p. 367–74. ISBN: 9788895940441.
- [20] Takeuchi E, Furuya Y, Nagashima N, Matsuoka S. The effect of frequency on the giga-cycle fatigue properties of a Ti–6Al–4V alloy. *FFEMS* 2008;31(7):599–605.
- [21] Jha SK, Szczepanski CJ, Johan R, Larsen JM. Deformation heterogeneities and their role in life-limiting fatigue failures in a two-phase titanium alloy. *Acta Mater* 2015;82:378–95.
- [22] Russian State Standard GOST-19807-91. Titanium and wrought titanium alloys; 2009.
- [23] Nikitin A. La Fatigue Gigacycle d'un alliage de Titane, PhD thesis, University-Paris Ouest Nanterre La Defense; 2015.
- [24] LeBlavand K, Pommier S, Prioul C. Local texture and fatigue crack initiation in Ti–6Al–4V titanium alloy. *Fatigue Fract Engng Mater Struct* 2003;25:527–45.
- [25] Nikitin A, Palin-Luc T, Shanyavskiy A, Bathias C. Crack path in aeronautical titanium alloy under ultrasonic torsion loading. In: Proceedings crack path 2012; 2015. p. 967–76.
- [26] Gates NR, Fatemi A. Crack paths in smooth and precracked specimens subjected to multiaxial cyclic stressing. *Frattura ed Integrità Strutturale* 2015;34:27–41. <http://dx.doi.org/10.3221/IGF-FSIS.34.03>.
- [27] Sonsino CM, Kaufmann H, Grubisic V. Transferability of material data for the example of a randomly loaded truck stub axle, SAE tech paper series, 970708; 1997. p. 1–22.
- [28] Nikitin A, Shanyavskiy A, Palin-Luc T, Bathias C. Fatigue behaviour of the titanium alloy Ti–6Al–4Mo in bifurcation area at 20 kHz. In: Proceedings '19th European conference on fracture' ECF-19, Kazan, Russia; 2012.

- [29] Nikitin A, Palin-Luc T, Shanyavskiy A, Bathias C. Influence of production process of Ti-6Al-4Mo titanium alloy on crack initiation mechanisms in VHCF regime. In: 6th international conference VHCF-6, Chengdu, China.
- [30] Shanyavskiy A. Fatigue cracking simulation based on crack closure effects in Al-based sheet materials subjected to biaxial cyclic loads. *Engng Fract Mech* 2011;78:1516–28. <http://dx.doi.org/10.1016/j.engfracmech.2011.01.019>.
- [31] Shiozawa D, Nakai Y, Murakami T, Noshio H. Observation of 3D shape and propagation mode transition of fatigue cracks in Ti-6Al-4V under cyclic torsion using CT imaging with ultra-bright synchrotron radiation. *Int J Fatigue* 2014;58:158–65. <http://dx.doi.org/10.1016/j.ijfatigue.2013.02.018>.